

Chapter 5

SUMMARY OF RESULTS AND A WAY FORWARD

Four primary flow modalities of multi-source wind tunnels have been discussed throughout this dissertation. In Chapter II, extensive visualizations of the uniform flow modality are introduced and serve as a baseline of comparison for the generation techniques to follow. In Chapter III, the generation of mixing layers through software partitioning was explored and the basic structure of dual- and triple-stream shear layers initiated across multi-source wind tunnels without the use of a splitterplate was established. Chapter IV marked the exploration of pseudo-random and quasi-coherent flowfields through the random-phase (R-P) and quasi-grid (Q-G) turbulence generation techniques, respectively. The fundamental objective of this work, indeed, is the experimental simulation of atmospheric-like disturbances, both continuous and discrete, from the perspective of the flyer near the surface in the presence of a reasonably strong wind. The suitability of the flowfields generated by multi-source wind tunnels as representative environmental forcing spectra were discussed in some depth and can be summarized by their research potential as:

- **Uniform flow** - a ‘passive’ grid-like turbulence useful for the study of classical (isotropic) turbulence with nominal $Re_{\lambda_T} = 135$, representing the baseline ‘conventional’ wind tunnel flow modality
- **Shearing flow** - splitterplate-less mixing layer(s) with locally isotropic turbulence in the layer interior with Re_{δ_ω} ranging from 4×10^4 to 4×10^5 ; a candidate experimental discrete gust forcing function provided the shear layer dynamics are decoupled from the flyer response dynamics as the flyer passes through
- **Pseudo-random flow** - random fluctuations about a targeted mean velocity with varying deviation amplitude that result in $500 \lesssim Re_{\lambda_T} \lesssim 900$, a good candidate for environmental forcing experienced far above local effects in the inertial sublayer (ISL)
- **Quasi-coherent flow** - more information regarding the spatial structure of these flowfields is warranted but can preliminarily be considered as a ‘greater-

diameter’ grid-like turbulence that generates a superimposed wake-like flow-field within the measurement domain with Re_{λ_T} routinely order 10^3 at relevant mean velocities, a principle development toward within-canopy type environmental forcing

Projecting forward, combinations of the above flow modalities may further unlock research potential (e.g. see appendix D for a preliminary overview of combining the shearing and pseudo-random flow modalities), but given the expansiveness of potential combinations afforded, candidate flowfields can only be systematically considered if an appropriate comparison framework is first established. Significant emphasis has been placed toward a spectral view, since the focus of testing narrows toward the energetic overlaps of the forcing spectrum and the natural modes of the flyers which can straightforwardly be analyzed through the energy spectrum. It is thus desirable for comparisons to be facilitated through a consistent spectral view for each of the flow modalities enabled through multi-source wind tunnels.

5.1 A framework for comparison

Though the flow types thus explored are markedly different, in any conceivable scenario of note, the flowfield encountered by the flyer is nearly always a high Reynolds number (high-Re) turbulent flowfield. It is this reality that enables a binding framework of comparison to be established. A quantitative definition of ‘high-Re’ is first given followed by a means with which to connect turbulence characteristics (i.e. representative length scales) to shearing velocity parameters, a useful scaling transformation considering that each of the flow modalities leverages shearing velocities of some kind at the array outlet to generate turbulent flowfields. A normalized spectral representation is then proposed as a quantitative metric to observe how the energy of the flowfield distributes amongst the frequency scales for the various flow modalities. Based on this spectral view, a few primary comparisons are discussed.

Fully-developed (post-transition) turbulence

The mixing transition criteria (Dimotakis, 2000) introduced in Chapter III, whereby the quality of the turbulence is observably different below and beyond, is restated here to serve as a quantitative definition for a sustained fully-developed turbulent flow field, or as a shorthand, a high-Re flow. For flowfields with appropriate outer scales, a high-Re flow must necessarily be, based on a bevy of experimental observation

for many different flow geometries,

$$Re = \frac{U\delta}{\nu} > 1 - 2 \times 10^4 \quad (5.1)$$

where U and δ are local values of the characteristic velocity that drive the turbulence in a flowfield of transverse extent, respectively. The Reynolds number for a region of the flowfield driven by a (constant) shearing velocity difference $\Delta U = U_2 - U_1$ across a transverse extent $\delta(x)$, as in the mixing layer cases, is defined then by

$$Re_{\Delta U} = \frac{\Delta U \cdot \delta(x)}{\nu} \quad (5.2)$$

For flow fields with no obvious or appropriate outer scales, the mixing transition criteria is defined by the Taylor microscale, λ_T , and the root mean square of the fluctuating velocity u' as:

$$Re_{\lambda_T} \equiv \frac{u' \lambda_T}{\nu} > 100 - 150 \quad (5.3)$$

Reynolds numbers exceeding these criteria are considered fully-developed, post-mixing-transition turbulent flow fields, or high-Re flows.

Indeed the notion of eddies of varying sizes within a turbulent flowfield is conceptualized from the picture of the turbulence cascade for fully-developed turbulence (stated generally as $Re_{\Delta U} \gg 1$ when derived). The three length scales of a turbulent velocity field describe eddies of the order of the shearing velocity transverse extent, eddies so small that viscosity dissipates energy as heat, and an intermediate range of eddies that transfers energy between the two, with each eddy convected by the local velocity vector. The dynamics of the energy-accepting larger scale eddies, denoted by extent λ_δ (which are of the order $\lambda_\delta \sim \delta$) are understood to essentially be inviscid. Thus, the rate at which these larger scale eddies acquire energy from the shearing velocity does not depend on viscosity, an idea first put forth by Taylor (1935). The energy is cascaded to smaller and smaller eddies under the influence of the strain field until they reach a small enough size for the effects of viscosity to dissipate the energy as heat. The smallest eddy scale, referred to as the Kolmogorov viscous scale, denoted λ_ν , acts as a limiting scale for the inviscid processes. Building on Taylor's ideas of inviscid scaling of larger eddies, Kolmogorov (1941) extended this rationale to eddies of size λ that are smaller than δ but still large enough such that their local eddy Reynolds number

$$Re_\lambda = \frac{u_\lambda \cdot \lambda}{\nu} \quad (5.4)$$

with a characteristic velocity u_λ associated with an eddy of extent λ is still larger than unity. Assuming that little to no energy is lost when transferring between ranges of inviscid eddies (i.e. the energy dissipation rate ε is constant), then

$$\varepsilon \sim \frac{u_\lambda^3}{\lambda} \approx \frac{\Delta U^3}{\delta} \quad (5.5)$$

is a useful approximation of an eddy of scale λ very nearly the size of the largest eddy δ . Plugging this approximation into eq. (5.4) and rearranging gives a relationship between the local eddy Reynolds number Re_λ and the turbulent shear flow Reynolds number as

$$Re_\lambda = Re_{\Delta U} \cdot \left(\frac{\lambda}{\delta}\right)^{4/3} \quad (5.6)$$

A threshold whereby viscosity can no longer be ignored would occur when the Reynolds number associated with a particular eddy is of order unity, i.e., $Re_\lambda = 1$. This occurs at eddies of scale λ_v whereby ?? gives under this condition

$$\frac{\lambda_v}{\delta} = Re_{\Delta U}^{-3/4} \quad (5.7)$$

The in-between characteristic length scale can further be defined for isotropic flow, whereby the dissipation rate ε and the volume-averaged velocity fluctuations u' are related by

$$\varepsilon = \frac{15\nu}{\lambda_T^2} u'^2 \quad (5.8)$$

where λ_T is the so-called Taylor microscale. With the ratio $u'^2/\Delta U^2$ constant for a fully developed turbulent flowfield due to a shearing velocity (see e.g. fig. 3.20 and fig. 3.21 to evaluate how well this assumption holds for multi-source-generated experimental shear layers), and assuming the dissipation rate ε scales with $\Delta U^3/\delta$ according to eq. (5.5), then Eq. eq. (5.8) can be rearranged to give a relationship between the length scale characteristic of the largest eddies δ , the length scale characteristic of the intermediate eddies λ_T and the Reynolds number defined for the region of the flowfield driven by a shearing velocity $Re_{\Delta U}$ as

$$\frac{\lambda_T}{\delta} = \gamma \cdot Re_{\Delta U}^{-1/2} \quad (5.9)$$

where γ is a constant of the flow.

The three length scales of a turbulent flowfield can then conveniently be expressed by the scaling relationships as follows

- The large eddy scale, $\lambda_\delta \sim \delta$

- The Taylor microscale, $\lambda_T \sim \delta \cdot Re_{\Delta U}^{-1/2}$
- The Kolmogorov scale, $\lambda_v \sim \delta \cdot Re_{\Delta U}^{-3/4}$

Moving amongst the scales

Each of these flow modalities as presented is united under the banner of high-Re flows and as such manifests a power-law regime of slope $\approx -5/3$ in the energy spectrum that should broaden with increasing Reynolds number. As will be made clear in subsequent analysis, it is useful to normalize eq. (4.1) by the total energy to give a fractional representation of the u-component energy per unit frequency at f as:

$$\int_0^{\infty} F_{11}(f) df = 1 \quad (5.10)$$

where $F_{11}(f) = E_{11}(f)/\overline{u'^2}$ and $F_{11}(f) \cdot df$ represents the fraction of the energy in the interval df at f . In this way, if the energy of the fluctuating components in the flow contains mostly large eddies, $F_{11}(f)$ will exist mainly in the region of low frequencies. If the energy of the fluctuating components in the flow contains mostly smaller eddies prone to dissipation, $F_{11}(f)$ will exist mainly in the region of high frequencies.

A useful comparison of the distribution of energy amongst the scales of various high-Re flows can be made through use of Raichlens criteria (Raichlen, 1967). In the normalized form of eq. (5.10), Raichlen proposed a demarcation of the particular frequency f_{50} at which exactly 50% of the energy of the fluctuating components is found above and below this value:

$$\int_0^{f_{50}} F_{11}(f) df + \int_{f_{50}}^{\infty} F_{11}(f) df = 0.5 + 0.5 \quad (5.11)$$

so that

$$\int_0^{f_{50}} F_{11}(f) df = 0.5 \quad (5.12)$$

Equation (5.12) is a useful criteria insomuch as this characteristic frequency has been observed to closely align with the transition from the large-scale energy region to the subinertial range (e.g., see Spencer, 1970, for the dual-stream mixing layer case) without reliance solely on sparsely collected data in the lower resolution region as $f \rightarrow 0$. Any such percentage can be targeted and found straightforwardly with numerical integration provided eq. (5.10) is (nearly) satisfied. A finite sampling

rate with data resolved according to Nyquist's criteria precludes characterizing energy contributions approaching infinity, though high frequency small eddy energy contributions are typically some four orders of magnitude or lesser than the large-scale energy accepting eddies found predominantly in the region $f < f_{50}$.

A criteria for the dissipative scales can likewise be determined. Hinze (1975) gives a spectral estimate of the Taylor microscale λ_{T_s} based on Taylor's hypothesis as

$$\frac{1}{\lambda_{T_s}^2} = \frac{2\pi^2}{U^2} \int_0^\infty f^2 F_{11}(f) df \quad (5.13)$$

Similar to the 50% criteria put forth to demarcate a 'beginning' of the inertial subrange, an estimate for the 'end' of the inertial subrange is made using the integral of eq. (5.13) as representation of the dissipative scale motion, so that

$$0.1 = \frac{2\pi^2 \lambda_{T_s}^2}{U^2} \int_0^{df_{10}} f^2 F_{11}(f) df \quad (5.14)$$

where df_{10} represents the dissipation frequency at which 90% of dissipative energy is found above this value (i.e. 10% is found below). If it is presumed that in some way the frequency df_{10} in eq. (5.14) demarcates frequencies above which energy contributes predominantly to dissipation processes for any given recorded observation (based on the notion that the Taylor microscale itself marks the length scale below which viscosity significantly affects the dynamics of the turbulent eddies), then a heuristic check of the validity of a fully-developed high-Re assumption can straightforwardly be made by looking for sufficient separation between energy-accepting and dissipative scales in the normalized spectral view. A [90% ←||→ 10%] demarcation at the frequency f_{90} can be used to mark an 'end' of a region where 90% of the total fluctuating energy resides. The [10% ←||→ 90%] demarcation at df_{10} is used to mark the 'start' of the dissipation contributing frequencies. Determination of these threshold frequencies partially reflects the choice of sampling frequency, as anything above the Nyquist frequency is susceptible to aliasing. If the two regions marked in this way are widely separated with no appreciable overlap, then an intermediate range of eddies is likely supported and statistical treatments that rely upon local isotropy are considered to be justified.

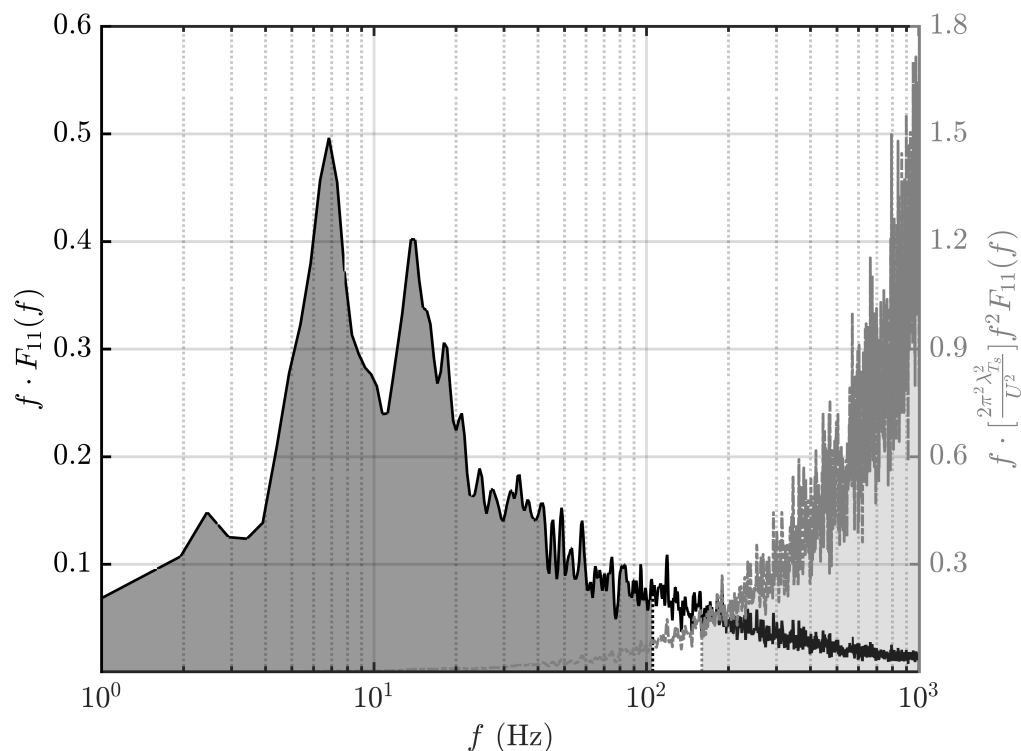


Figure 5.1: Normalized energy spectrum plotted in an area-preserved manner highlighting two separate and non-overlapping regions. The leftmost region demarcates the frequencies that contribute 90% of the total fluctuation energy (from $f \rightarrow 0$ to f_{90}) and the rightmost region reflects the frequencies that account for 90% of the energetic contribution to dissipative processes (from df_{10} to $f_s/2$, where f_s is the sampling rate).

Interpreting with caution

With these analysis techniques now established, comparisons between primary flow modalities can cautiously be made. Because shearing velocities initiated at the fan array outlet plane are the primary mechanism by which the turbulent flowfields evolve, greater focus has been placed on the nearly inviscid dynamics of the large energy-accepting eddies. However, as previously shown, advantages in analysis emerge when considering the cascade of energy through the intermediate range of eddies down to the dissipative scales. Canonical treatments used to fit a form of the energy spectrum based on the $-5/3$ behavior of the intermediate range, though useful, presume a single length scale attributed to the large energy-accepting eddies. Noticeable multi-scale behavior is present, for example, in the quasi-grid (Q-G)

initiated flowfield of fig. 5.1 and scaling techniques presuming a primary time or length scale are likely to miss (i.e. smooth) the discrete contributions of the forced (and not necessarily equal) intergrid spacings.

Further care must be exercised for instances when a frequency component with a period longer than the record length is present, as the presence of a ‘trend’ in the time series renders the data nonstationary. Trend removal is beyond the scope of discussion, but suffice to say that selection of relatively short record lengths ($T = 32\text{s}$ or 64s) and limitation of the range of forcing frequencies to $f_p > 0.05$ Hz eliminates all long-lasting trends except that of the purely sinusoidal flowfields of the ‘breathing’ modality (which have been omitted and left to future careful study). Flow-induced oscillations from the quasi-coherent evolvments of the coarsening grid-like RPM distributions, though in some cases discretely energetic, are not considered ‘trends’ in the sense previously described and are thus included when calculating $\overline{u'^2}$. This reflects the notion that natural shear layer evolutions discretely separated at initiation and their subsequent downstream mergings are considered fundamentally differently than are artificially forced input oscillations of a ‘breathing’ modality. The pseudo-random flows initiated by the random-phase (R-P) algorithm conceptually represent something sitting in-between the aforementioned, but the results in appendix C support that energy is added broadly across frequency scales with no preference toward any obvious (discrete) frequency thus contributing to u' and included in the calculation of $\overline{u'^2}$, when applicable.

It is perhaps a bit clearer now, with these cautions made explicit, the appeal of a statistical metric that does not presume a certain form of the correlation function(s) in the low-wavenumber regions. The spectral representation of the dissipative scales in eq. (5.13), unlike eq. (5.12), does assume a form, but its application is limited to the range of scales well-supported to behave universally with a constant dissipation rate and is merely used as a ‘sanity-check’ for the separation of scales assumed for high-Re flows. More central to this analysis are characteristic time and length scales associated with the various inviscid flow dynamics enabled through the multi-sourcedness of the fan array. In general, homogenous and isotropic assumptions are required to express measured Eulerian turbulence characteristics in some physically meaningful way. Of course an incompressible turbulent shear flow subjected to a mean deformation rate, as in the mixing layer case, is very much so anisotropic with a continuous production of turbulence due to the mean shear. Likewise Taylor’s

hypothesis regarding the spatial structure of turbulence essentially remaining unchanged when carried along by a mean velocity must be carefully considered when neither the main flow is uniform nor the level of turbulence low. The applicability of Kolmogorov's and Taylor's hypotheses for a shear flow were explored by Hinze (1975) and Lin (1953), respectively. Their findings can be summarized in terms of time scales present in the flow. When the time-scale of the changes of the statistical parameters are small compared to the time-scale of the turbulent fluctuations and when the main motion is steady (i.e. without 'trends'), averages taken with respect to time can be justified if the production of energy nearly compensates for its dissipation. According to Lin's criteria, Taylor's hypothesis is valid for shear flows when

$$f \gg \frac{1}{2\pi} \frac{\Delta U}{\delta_\omega} \quad (5.15)$$

providing further justification of the universality of the turbulence cascade beyond the inviscid region. What remains, then, is classification of the large energy-accepting regions which will be accomplished through use of the semi-arbitrary frequency threshold f_{50} . An estimate of the integral length scale in the longitudinal direction is calculated from

$$Lu_x = \frac{1}{2\pi} \frac{U_c}{f_{50}} \quad (5.16)$$

where U_c is the convective velocity of the initial shear layer(s) at the fan array outlet plane taken roughly equivalent to the average of the two outer streams (or wake/non-wake regions).

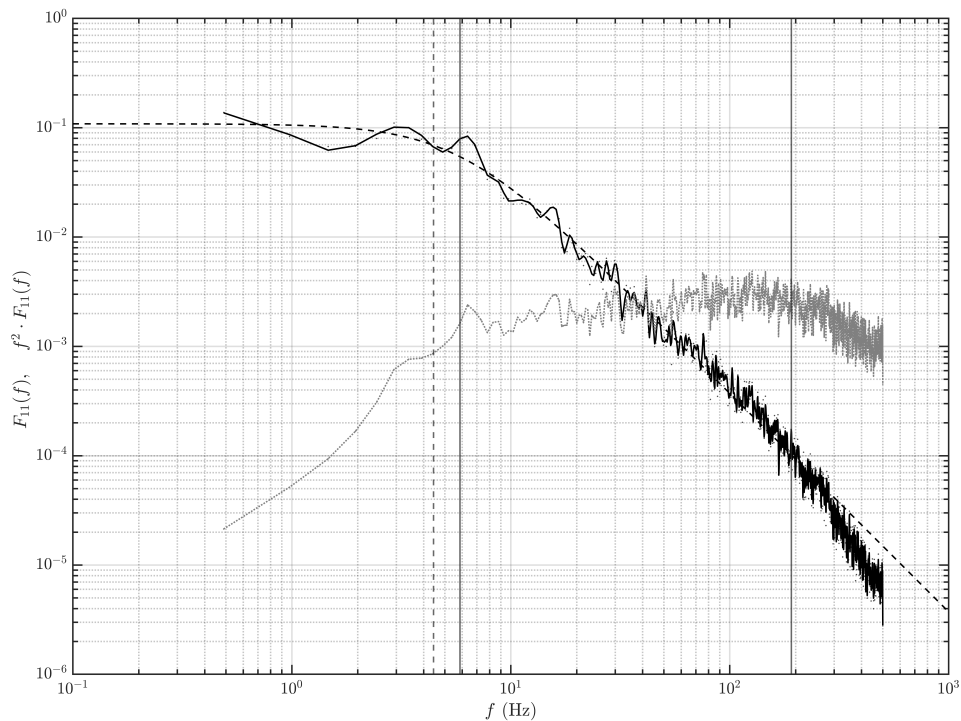


Figure 5.2: Normalized energy spectrum for $r = 0.2$ along the centerline at $x = 118$ inches. The dashed vertical line marks the frequency of validity according to Lin's criteria. The left-most solid vertical line marks the Raichlen criteria of f_{50} and gives a reasonable estimate of the beginning of the $-5/3$ roll-off. The right-most solid vertical line marks df_{10} and reasonably divides the frequency at which the slope steepens away in the dissipative range. The theoretical fit is of a form proposed by Dryden.

5.2 Comparisons

General behaviors amongst the modalities are now considered by comparing the statistical markers derived from the normalized spectral view. A representative example is provided in fig. 5.3 through comparison of the uniform flow modality, quasi-grid flow modality, and the centerline of a dual-stream mixing layer in the wavenumber domain.

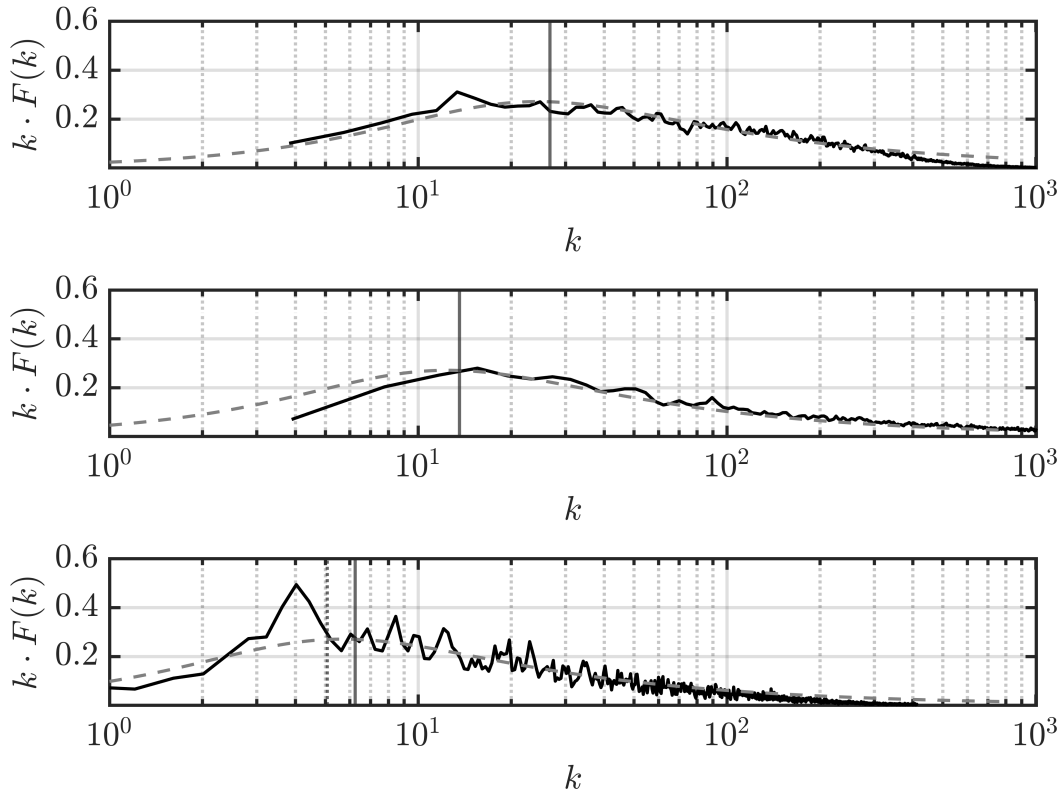


Figure 5.3: Normalized energy spectrum for the uniform flow modality (top), the quasi-grid modality (middle), and dual-stream shear layer $r = 0.2$ along the centerline (below), each at $x/L \sim 0.75$. The solid vertical line corresponds to the wavenumber based on f_{50} . The dashed vertical line of the dual shear layer normalized energy spectrum corresponds to Lin's criteria.

The areas under the F_{11} curves integrate to unity within 5%. Various theoretical forms of the function F_{11} have been proposed, with Kolmogorov's theory for isotropic homogenous turbulence describing the cascade of energy through the dissipative scales ubiquitously used and validated for a wide range of turbulent flows. The form proposed by von Kármán in eq. (1.11) is dashed when included and is expected to be a reasonable fit beyond the criteria of eq. (5.15). The solid vertical lines of fig. 5.3 correspond to $k_{50} = 2\pi f_{50}/U_c$. The maximum linear wavelength associated with the inverse wavenumber contributing 50% of the energy is then $\Lambda_x^u = 2\pi/k_{50}$.

Table 5.1: Summary of results tabulated using Raichlen’s criteria for three different flow modalities at approximately the same measurement location.

Type	x (in)	f_{50} (Hz)	Lu_x (in)	Λ_x^u (in)
Uniform	92	34	1.5	9.3
Quasi-coherent	92	17	2.9	18.2
Dual-stream ML	88	8	6.3	39.6

With the baseline uniform flow modality statistically established in table 5.1, it is clear that the effect of coarsening the RPM distribution of the fan array outlet plane into a quasi-grid and dual-stream mixing layer shifts energy into lower wavenumbers accordingly. A module related funneling effect was discussed in detail in section 2.2 and appendix B. For the uniform flow modality, Λ_x^u is 9.3 in. (0.235 m), corresponding to the distance between module-center peaks (i.e. $3d$, $d = 0.080$ m) of the velocity profile (see fig. 2.5). Aside from this funneling effect, there is no significant ΔU at the fan array outlet plane and a canonical form of the energy spectrum yields a good fit. The module funneling effect was also noted in the outer freestreams of the mixing layers and is likely present in some form in the quasi-grid configuration (though traverses have yet been carried through to confirm).

Along the centerline interior of the dual-stream mixing layer, the dominant wavelength is expected to be the streamwise coherent structure spacing Λ_x . Using the estimate from k_{50} , values for $\Lambda_x^u/\delta_\omega$ can be calculated based on the previously presented results of Chapter III. Table 5.2 shows that the estimate of the streamwise spacing normalized by the vorticity thickness is well within the range $3.1 < \Lambda_x/\delta_\omega < 5.0$ reported in the literature for dual-stream mixing layers (Dimotakis and Brown, 1976), further lending credence to the utility of the 50% energy threshold. Interestingly, the average of f_{50} for the upper and lower triple-stream mixing layer initially separated by $ss = 4d$ and allowed to evolve is essentially the value of f_{50} calculated for the $r = 0.2$ dual-stream mixing layer, suggestive that the separated triple-stream mixing layers are energetically similar (when normalized) and redistribute energy upon merging centered about the average of their previous respective characteristic frequencies. The R-P modality appears, at first take, to be the obvious perturbation candidate when uniformity is to be maintained but significant ‘roughening’ of the flow is enabled through static reconfiguration (i.e. ‘coarsening’) of the RPM input distribution and this yields significant increases in the fluctuating energy. Further traverse-based testing is warranted for the quasi-coherent flow types in light of the comparison framework.

Table 5.2: Summary of results tabulated using Raichlen’s criteria for a dual-stream and triple-stream mixing layer.

r	x (in)	f_{50} (Hz)	Lu_x (in)	$\Lambda_x^u/\delta_\omega$
0.16	28	19	2.4	3.6
0.18	58	-	-	-
0.19	88	8	6.3	3.7
0.19	118	6	7.9	3.5
r_{upper}	x (in)	f_{50} (Hz)	Lu_x (in)	$\Lambda_x^u/\delta_\omega$
0.34	28	28	2.1	3.3
0.43	58	18	3.2	3.5
0.48	88	11	5.2	4.1
-	118	9	6.6	-
r_{lower}	x (in)	f_{50} (Hz)	Lu_x (in)	$\Lambda_x^u/\delta_\omega$
0.34	28	9	3.3	4.1
0.43	58	8	3.4	3.0
0.48	88	5	5.7	4.0
-	118	3	8.5	-

5.3 Concluding remarks

The qualitative behavior of the turbulence is observably different when fully-developed post-mixing-transition. For all the flow modalities thus far presented, the high-Re number criteria ($Re_\delta \approx 10^4$, $Re_{\lambda_T} \approx 10^2$) has been met. This serves, then, as a necessary minimum requirement in the development of multi-source wind tunnels with intended use as environmental simulators for flyers near the surface. Characteristics of the evolving flowfields can further be tuned through the introduction of perturbation techniques applied as initial conditions.

The uniform flow modality (i.e. all fan units set to produce nominally the same initial velocity condition) develops a well-mixed (within 2% of the mean) turbulent flowfield beyond $x/L \sim 0.5$ with $Re_{\lambda_T} = 135$ and serves as a basis of comparison for all other flow modalities discussed herein. Both initialized dual-stream and triple-stream mixing layers at flight-relevant freestream velocity differences are explored and found to principally behave like the mixing layers developed in a more conventional splitterplate experiment. The Reynolds number Re_{δ_ω} based on the velocity difference ΔU and vorticity thickness δ_ω (both outer scale parameters) is shown to linearly increase with downstream development as the vorticity thickness increases commensurately. The spectral analysis along the centerline confirms local isotropy for every tested case. Statements of the *suitability* of these mixing layers as experimental forcing functions for discrete gust testing can only be made with the

(approximate) flyer dynamics known. That is to say that the coupling/non-coupling of dynamics (length scales, frequency scales, etc.) between the environment and the flyer is determined by the flyer dynamics in relation to the generated shear layers. At least qualitatively the ‘right’ kind of mixing layer (i.e. fully-developed at relevant freestream velocities) is created within the testing envelope of the multi-source wind tunnel that serves as a candidate flow modality to be used in discrete gust experiments for full-scale dynamic vehicle testing.

The random-phase perturbation technique proves useful in increasing Re_{λ_T} upwards of nearly sevenfold with only a slight further-loss-of-uniformity (to within 3.7% of the mean). Significant increases in Re_{λ_T} are made through a static-reconfiguring of the discrete source fan-units into a so called quasi-grid flow modality. The highest recorded Taylor microscale Reynolds number was found to be $Re_{\lambda_T} = 2700$, likely accompanied by a non-negligible loss of uniformity at the fixed measurement location, though traverses were not undertaken during this campaign so no direct statement of homogeneity is put forth. Each flow modality is shown through the presence of a -5/3 slope power law region to be locally isotropic at relevant freestream velocities with an inertial subrange that dilates further as Re_{λ_T} increases.

5.4 Looking forward - research potential

Development of a multi-source wind-generating apparatus that produces relevant mean velocities and appropriate high-Re flowfields in an ample (and open) test envelope primes its use as an environmental flow simulator for near surface flowfields. Further to the point, appropriate and useful (i.e. machine-learning-capable¹) free-flight full-scale autonomous (manmade and/or natural) vehicle testing is made possible. For a brief overview of two-such facilities (CAST at Caltech and a temporary takeover of the 25ft Space Simulator at JPL to assist in the forward flight characterization of the Mars helicopter Ingenuity), see appendix A.4.

It is thought that the development of a large and open multi-source wind tunnel test facility further provides significant research potential toward the more fundamental understanding of the development of turbulence through shearing velocities. In time, with higher resolution traverses and flow visualization techniques further developed, questions surrounding the treatment of flowfields post-mixing transition may be better understood. For instance, in the case of the mixing layer, significant controversy still remains as to whether the initialized quasi-2D coherent structures

¹‘crash and learn’, as davidkremers says.

that grow pre-transition from pairing events continue to do so two-dimensionally post-mixing-transition. Numerical discrepancies at high-Re center squarely upon this matter (e.g., cf. McMullan et al., 2015; Suryanarayanan and Narasimha, 2017). The artifice of the wake of the splitterplate in the development of mixing layers is obviated (or at least reduced in a spanwise-coherence sense) through replacement of the splitterplate geometry with a software-based static reconfiguration of many discrete source fans and, because the testing domain is open-air, influences from artificial solid boundaries occur significantly further downstream.

Moreover, it is believed that some of the significant freestream nonuniformities that result from the multi-source module design can be reduced with careful software calibration, conventional flow-manipulator introduction, or by simply shifting testing further downstream, provided the envelope allows for it. Further solace is found in the consideration that local isotropy is observed in each primary flow modality, so that the details of the largely inviscid dynamics of the low wavenumber range eddies do not fundamentally alter the cascade of energy in the inertial subrange down to the dissipative scales.